Erschienen in: 29th European PV Solar Energy Conference and Exhibition : proceedings of the international conference held in Amsterdam, The Netherlands, 22 - 26 September 2014 / realised by: WIP...; ed. by: T. P. Bokhoven... (Hrsg.). - München : WIP, 2014. - S. 427-432. - ISSN 2196-100X. - ISBN 3-936338-34-5
https://dx.doi.org/10.4229/EUPVSEC20142014-2BO.2.5

TEMPERATURE DEPENDENCE OF VOID FORMATION IN PERC CELLS AND THEIR SPATIALLY RESOLVED DETECTION BY COMBINING SCANNING ACOUSTIC MICROSCOPY AND ELECTROMLUMINESCENCE MEASUREMENTS

Renate Horbelt[1], Axel Herguth[1], Giso Hahn[1], Reinhart Job[2], Barbara Terheiden[1]
[1]University of Konstanz, Department of Physics, 78457 Konstanz, Germany
[2] Münster University of Applied Sciences, Dep. of El. Engineering and Computer Science, 48565 Steinfurt, Germany
Author for correspondence: renate.horbelt@uni-konstanz.de, Tel.: +49 7531 884995, Fax: +49 7531 883895

ABSTRACT: Key aspect of this work is the investigation of local Al contacts with regard to void formation under a non-uniform temperature of the solar cell during the firing process in the belt furnace. The impact on electrical properties is determined by IV measurements and electroluminescence imaging (EL). Scanning acoustic microscope (SAM) measurements on full cell area are used for a spatially resolved localization of voids. Combining all these characterization techniques, the impact of thermal non-uniformity on contact formation can be determined spatially resolved. Furthermore, a detailed investigation of BSF thickness of two different Al-pastes shows a clear correlation with temperature distribution on the wafer during the co-firing process. All results demonstrate the importance of a well optimized Al-paste and an absolutely uniform temperature on the Si wafer for an excellent formation of local rear contacts.
Keywords: Screen Printing, Local Contact, Back-Surface-Field

1 INTRODUCTION

Passivated Emitter and Rear Contact (PERC) solar cells feature local contacts to the solar cell base on the rear side. The contacts are conventionally established using Al-paste on top of a locally opened passivating dielectric layer. The local contact formation is based on (i) melting of the Al matrix, (ii) dissolution of Si at the solid Si / liquid Al interface, diffusion of Si into the Al-paste matrix and in consequence carving of the silicon bulk, (iii) recrystallization of Si doped up to the solubility limit with Al above the eutectic temperature and (iv) solidification of the remaining Al:Si alloy at the eutectic temperature according to the binary phase diagram of Al and Si [1].

Ideally the local contact features an eutectic layer and a uniformly distributed Local Back Surface Field (LBSF). However, under certain conditions this eutectic layer is not formed and the local contact remains unfilled after the firing process. This unfilled contact is well known in literature as void. In such a case the LBSF can show reduced thickness or is completely lacking.

A lot of investigations regarding the local contact formation as well as the formation of voids have been carried out so far. These studies focused on the impact of the composition of the paste matrix [2], the contact geometry [3-5], the firing parameters [6, 7], the diffusion process of Si [8, 9], the contact opening techniques [10, 11], or the post laser treatment [12]. However, up to now the void formation is not completely understood.

In general the detection of voids is carried out by Scanning Electron Microscopy (SEM). This method needs a high effort for sample preparation in particular for void detection by cross sectional images. Since this technique is usually limited to a few cross-sections and thus small areas, only little information is gained regarding the spatial distribution of voids on large areas as full industrial solar cells.

The implementation of Scanning Acoustic Microscopy (SAM) as a characterization technique circumvents the above mentioned drawbacks of SEM. A comparison of SEM and SAM analysis has confirmed that SAM is an adequate alternative for the detection of voids [13].

Key aspect of this work is the investigation of local contact formation with regard to void formation in dependence of a non-uniform temperature of the solar cell during the firing process in a belt furnace. The impact on the electrical properties is determined by IV measurements and electroluminescence (EL) imaging. Dressler et al. [13] have shown the accordance of SEM and SAM on small cell areas. Within this work for the first time SAM measurements are used for a spatially resolved localization of voids on full cell area. Combining these characterization techniques, the impact of thermal non-uniformity onto contact formation can be determined spatially resolved.

Another aspect within this work is the investigation of two different Al-pastes and their dependence on the non-uniform temperature treatment in a belt furnace with regard to LBSF and void formation. The resulting LBSF layer thickness is investigated by SEM and correlated to the temperature distribution on the wafer during the co-firing process.

2 EXPERIMENTAL DETAILS

2.1 Scanning Acoustic Microscopy (SAM)

The measurement setup consists of a transducer which converts an electrical signal into an acoustic signal. The emitted ultrasonic waves are focused and transmitted to the solar cell by the coupling medium (deionized water). The interaction of the ultrasonic waves with the different materials and surfaces of the investigated solar cell leads to a reflection and scattering of the incoming wave. Only the reflected signal is detected by the transducer and converted back to an electric signal. The amplitude, phase and time of flight of the reflected signal are analyzed. A pixel-by-pixel image of the scanned solar cell is created revealing the voids in the local contacts.

2.2 Temperature profiling

For determination of the exact temperature deviation along the sample, two thermocouples were fixed on the front side of the sample connected with a temperature tracker. Each thermocouple was located at a distance of

~1.5 cm to the wafer edge at the front and rear end.

A test sample (detailed description see section 2.3) without front side grid is used. Due to this cell-like sample structure the thermal load of the wafer and in particular the contact area is comparable to "real cells". The firing parameters are adapted in a way that a temperature gradient within one sample is detectable.

Fig. 1 shows an example of a temperature profile recorded by the temperature tracker. The firing parameters are: (i) a deviation ($\Delta T_{standard}$) to the "standard set temperature of the furnace" of 40°C and (ii) a "reduced" belt speed (v_{belt}). The detected temperature difference between the sample front and rear edge is 25°C at peak temperature (T_{peak}). All firing profiles listed in Table I show such a temperature deviation of 25°C on the wafer.

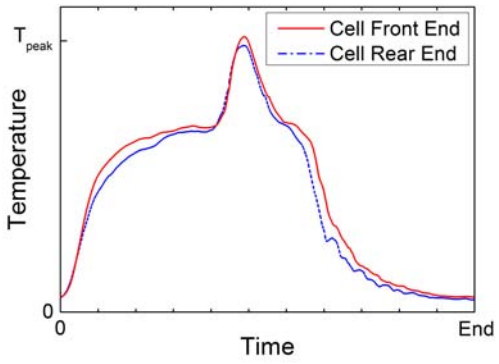

Figure 1: Thermal profile recorded with a temperature tracker during contact firing of the samples in a belt furnace.

Table I: Variation of the applied firing parameters.

$\Delta T_{standard}$ [°C]	-80	-60	-40	0	0
v_{belt}	reduced			std.	acc.
Paste 1	X	X	X		
Paste 2		X	X	X	X

2.3 Device Processing Sequence

For these experiments p-type Czochralski (Cz) Si wafers (2-3 Ωcm, 125x125 mm^2, ~170 µm) are used. After single side texturization a wet chemical cleaning step and a homogenous n^+-emitter $POCl_3$ diffusion (60 Ω/sq) is carried out. The P-glass is removed in HF solution subsequently followed by RCA cleaning and thermal oxidation. The thin thermal oxide layer on the front side is covered by a hydrogenated SiN_x:H layer via plasma-enhanced chemical vapor deposition which serves as an anti-reflection coating. In addition, the SiN_x:H layer serves as an etching barrier for the removal of the oxide layer and the emitter on the rear side. Therefore, the layer thickness is chosen to withstand the following wet chemical cleaning steps. The dielectric stack on the rear side consists of a 10 nm thin Al_2O_3 layer (atomic layer deposited) covered by a 120 nm thick hydrogenated SiN_x:H layer (remote PECVD). The local contact openings are structured by a ps pulse laser. The pattern applied to the dielectric layer stack consists of three different line widths (40 µm, 60 µm, 80 µm) at a constant pitch of 1.1 mm. This pattern allows the investigation of the void formation depending on line width. The front side grids of all wafers are screen printed with a commercially available Ag paste (finger width ~100 µm). For the screen printing of the rear contact two different commercially available Al pastes (pastes 1 and 2) are used. The samples are subdivided in several groups to vary the firing parameters (see Table I).

After co-firing of the contacts and edge isolation with a dicing saw all cells are characterized. Electrical parameters are determined by IV and EL measurements. A spatially resolved detection of the void formation is carried out by SAM mappings. LBSF layer thickness is determined by SEM.

3 RESULTS AND DISCUSSION

3.1 IV Measurement Data

Fig. 2 shows the measured fill-factors (FF) and open circuit voltages V_{oc} of the processed solar cells. Paste 1 exhibit excellent values independent of the firing parameters. The FF values of cells processed with paste 2 are on a significantly lower level.

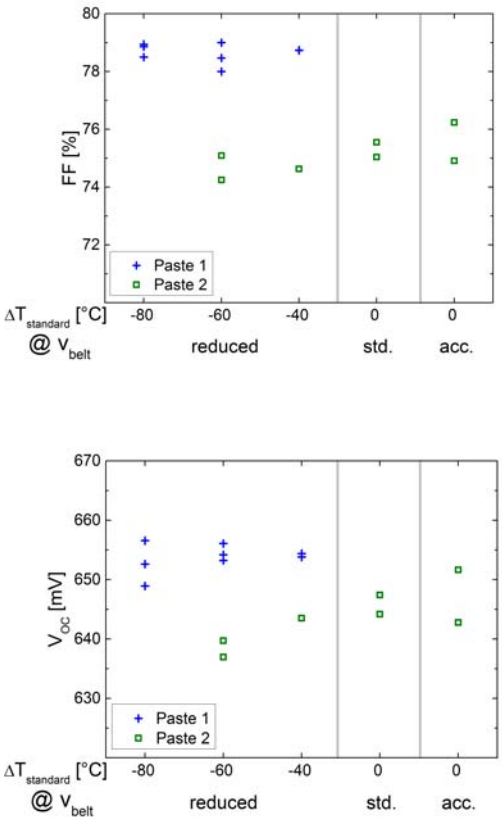

Figure 2: IV parameter of the processed solar cells. The cell area after edge isolation is 110.25 cm^2.

3.2 Comparison of EL and SAM Measurements

In Fig. 3 two characteristic SAM images are shown. Note that the screen-printed front side grid lines run perpendicular to the rear side fingers in order to separate the signals of front and rear from the EL and SAM measurements. The thin (horizontal) dark lines indicate voids in the local rear contacts. The thick horizontal lines are the front side busbars and the angled lines on the edges originate from the sample mounting. The green arrow denotes the direction the wafer moves in the belt furnace. The rear contact openings with a width of 40 µm

are at the bottom, 60 µm in the centre and 80 µm at the top region of the cells as indicated in Fig. 3. Note that all EL and SAM images are arranged in this way.

Both cells are processed at identical firing conditions (T_{peak} = -40°C, v_{belt} = "reduced"). Both pastes lead to a high amount of voids. Neither the opening width of the rear contacts nor the temperature gradient of 25°C have a significant impact on the void formation.

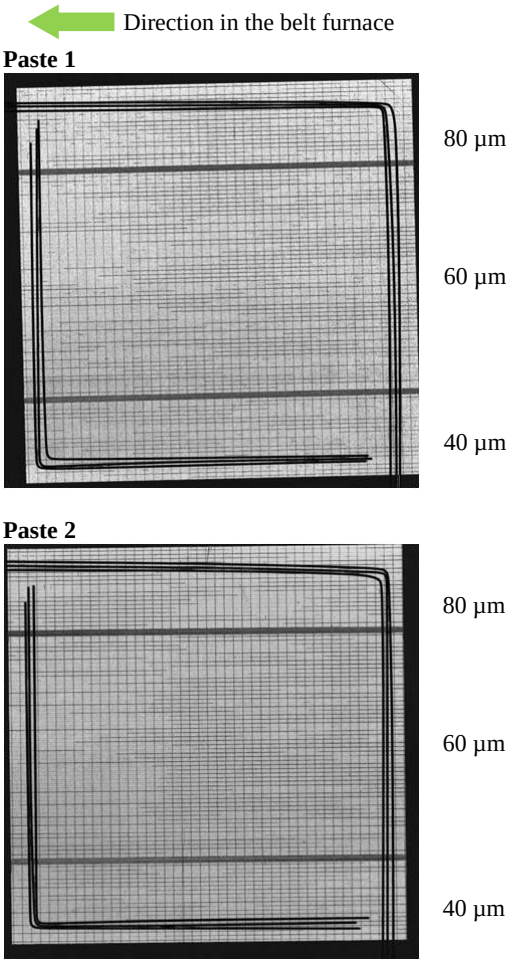

Figure 3: SAM measurements of two different solar cells fired with identical parameters (T_{peak} = -40°C, v_{belt} = "reduced").

Fig. 4 shows the corresponding EL images. The cell with paste 1 shows a quite homogeneous EL signal. Only at the cell rear end a small decrease of EL signal intensity is detectable. This is in agreement with the IV parameters of the cell indicating that the electrical parameters of the solar cells contacted with paste 1 are not negatively affected by the high amount of voids.

The EL image on the cell with paste 2 shows a significantly different behavior: the overall intensity is lower than the intensity of the cell with paste 1 (note the different scaling). Once again this is in agreement with the IV parameters of this cell. In addition, the intensity of the EL signal is lower at the rear edge of the cell, indicating a significant temperature dependence of the contact formation process of this paste to Si. The EL signal intensity in the areas with the 40 µm contact width (bottom of the cell) is lower than in regions with opening widths of 60 µm and 80 µm. To explain this phenomenon, the LBSF thickness on the front and rear end of cells processed with paste 1 and paste 2 is investigated in detail (see section 3.3).

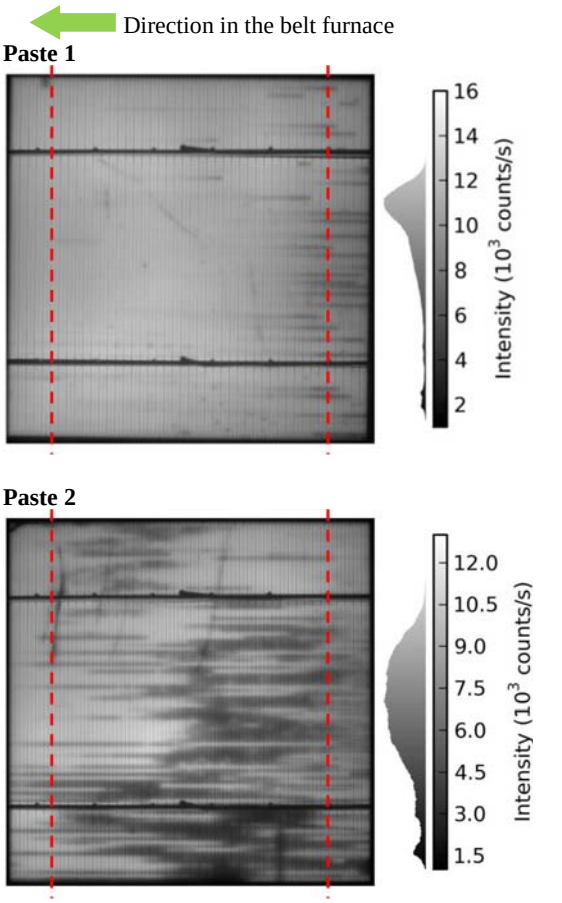

Figure 4: EL measurements corresponding to the two solar cells shown in Fig. 3. All measurements are carried out at a current density of 30 mA/cm^2. Note the different scaling of the intensity. The dashed lines symbolize the breaking edge for the investigation of the LBSF thickness by SEM images.

An additional phenomenon for paste 2 is shown in Fig: 5. The temperature dependence of the void formation is increased for "standard" firing conditions compared to T_{peak} = -40°C, v_{belt} = "reduced". Applying these firing parameters, the EL image as well as the SAM image indicate a significant temperature dependence. This is visible in a lower signal intensity at the sample rear end of the EL image and a higher amount of voids on the rear end of the sample in the SAM image.

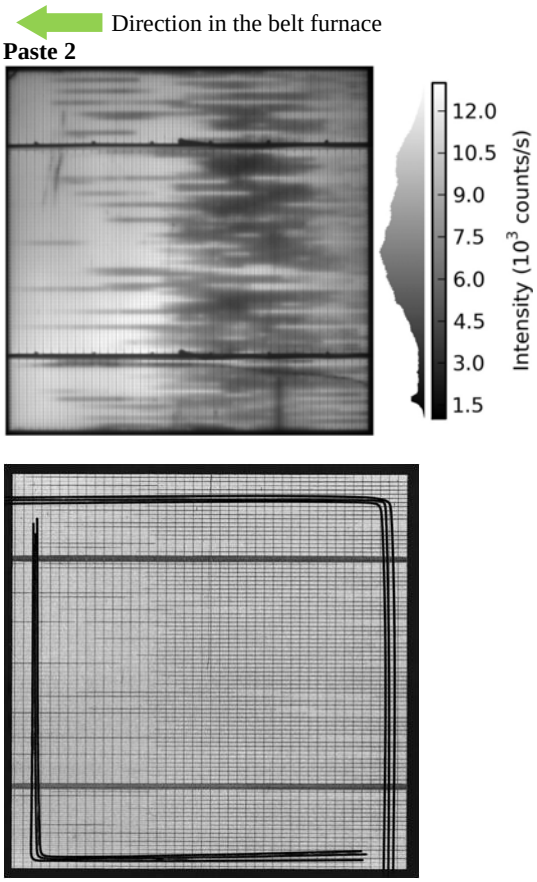

Figure 5: EL image (on top) and SAM image (bottom) of a cell processed with paste 2. "Standard temperature" and v_{belt} = "standard" are applied for the firing of this cell. A clear increase of voids on the rear end is detectable.

3.3 Characterization of local contact formation by SEM

Two cells under investigation are processed applying the same firing parameters as the cells shown in Fig. 4. To get a sufficient statistic, 220 contacts on each cell are investigated in terms of contact type (filled contact or void) and LBSF thickness. The dashed lines in Fig. 4 show where the wafer was broken at 1 cm distance to the front and the rear end, respectively. Since the wafer was broken perpendicular to the rear contact openings the cross-sectional view allows a quantitative determination of the LBSF thickness by SEM. Fig. 6 shows a filled contact and a void, the red lines indicate the spots where the LBSF thickness was determined (LBSF appears bright in the SEM images). An average of both values of the LBSF is taken for the analysis.

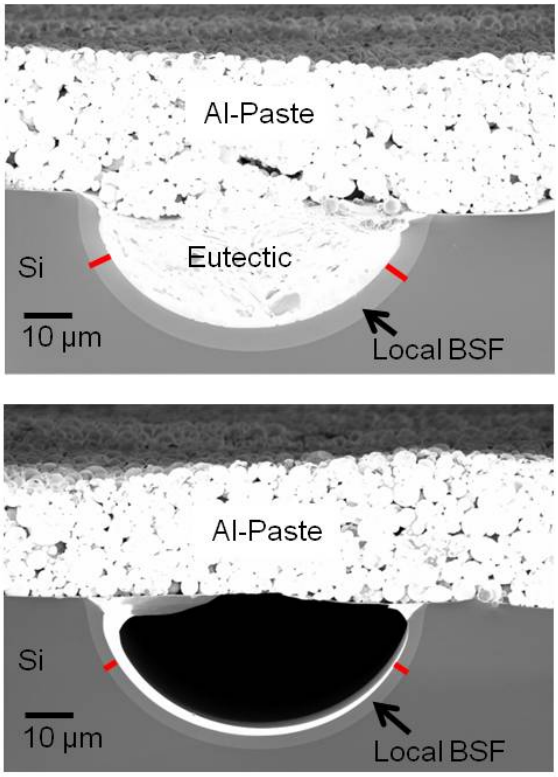

Figure 6: SEM images of local contacts with a contact opening width of 40 µm. The upper one shows a filled contact, the lower one a void. For the analysis of the LBSF thickness the average value of the left and right side is used (indicated by the red line).

3.3.1 LBSF thickness of filled contacts

Fig. 7 summarizes the results of LBSF thickness of all filled contacts on the front and rear end of the cells. A homogeneous LBSF is formed in all contacts. The average LBSF thickness of *paste 1* is higher than – or at least as high as - for paste 2. This correlates well with the EL measurements indicating a higher signal intensity thus a lower recombination for cells processed with paste 1. The LBSF thickness of paste 1 on the front end increases from 40 µm to 60 µm openings. On the cell rear end the LBSF thickness of paste 1 is on a constant level independent of the contact opening width.

The LBSF thickness of *paste 2* shows for the front and rear end a marginal increase with increasing contact opening width. This is in accordance with the EL measurements indicating a reduced signal intensity for the 40 µm contact openings for paste 2.

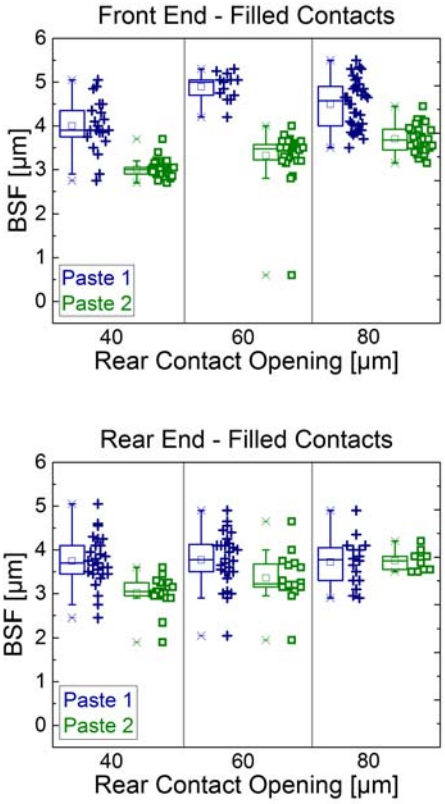

Figure 7: LBSF layer thickness of all filled contacts detected on the front end and on the rear end of the cell.

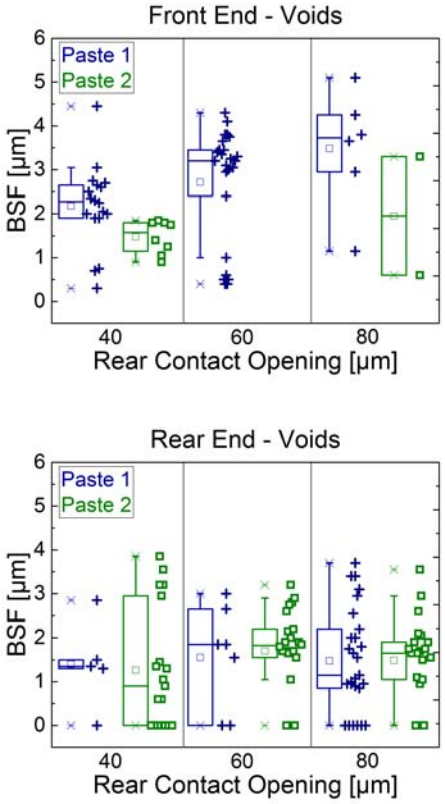

Figure 8: LBSF layer thickness in all voids detected on the front end and on the rear end of the cell.

3.3.2 LBSF thickness in voids

All detected voids (see Fig. 8) at the front end show at least a very thin LBSF. Once again the average LBSF thickness of *paste 1* is higher than the LBSF thickness of paste 2. Paste 1 shows more voids at the cell front end than paste 2. For *paste 2* no void is visible for 60 µm contact openings and just 2 voids are visible on 80 µm openings.

On the cell rear end the amount of voids for *paste 2* is higher than for paste 1. For both pastes a lot of voids are characterized by a totally missing LBSF layer, independent of the contact opening width.

Two main aspects have to be pointed out:

(i) Even if there is a large variation in LBSF thickness, the average value of the LBSF thickness on the rear end is in total smaller than on the front end. Once again these results fit well with the EL measurements and can be attributed to the lower temperature at the rear end.

(ii) Comparing the LBSF thickness of filled contacts (see Fig. 7) with that of all detected voids (see Fig. 8), it becomes obvious that filled contacts have a thicker LBSF than voids. These measurements confirm the results of Meng et al. [14] who showed thinner LBSF layers for partly filled contacts. Lauermann et al. [9] and Fang et al. [15] assume thinner LBSF layers for voids compared to filled contacts.

4 CONCLUSION

In this work it is shown that both investigated commercially available Al-pastes lead to a high amount of voids independent of the applied firing temperature and belt speed. The impact on the electrical cell parameters is directly correlated to the LBSF formation in the local contacts. This is verified by a detailed study of the LBSF thickness on two cells processed with the same firing parameters. All investigated filled contacts feature a LBSF of several micrometers. The LBSF of filled contacts is thicker than the LBSF of voids. A clear temperature dependence is detectable in terms of a thinner or totally missing LBSF layer in the voids on the cell rear end. This is attributed to a lower firing temperature at the rear end, which is verified by temperature measurements with thermocouples on the cell.

A lower overall EL signal intensity of paste 2 can be clearly attributed to a thinner local BSF. Furthermore, paste 2 shows another phenomenon: increasing the belt speed and firing temperature leads to a strong dependence of the void formation on the thermal gradient over the wafer.

The width of the locally opened rear contact does not have an impact on the void formation, but on the formation of the local BSF layer. For the pastes under investigation a wider rear contact opening leads in most cases to an increase of the LBSF thickness.

All results demonstrate the importance of a well optimized Al-paste and an absolutely uniform temperature on the Si wafer for an excellent formation of local rear contacts.

ACKNOLEDGEMENTS

Part of this work was financially supported by the German Federal Ministry for the Environment, Nature Conservation and Nuclear Safety (FKZ 0325581). The content is the responsibility of the authors.

The authors would like to thank K. Dressler, J. Engelhart, S. Fritz, L. Mahlstaedt, F. Mutter, S. Riegel and A. Zuschlag for their support.

REFERENCES

[1] J. L. Murray and A. J. McAlister, *Bulletin of Alloy Phase Diagrams* 5 (1984) 74.
[2] M. Rauer, C. Schmiga, R. Woehl, K. Rühle, M. Hermle, M. Hörteis, D. Biro, S. W. Glunz, IEEE J. PV 1 (2011), 22.
[3] E. Urrejola, K. Peter, H. Plagwitz, G. Schubert, J. Appl. Phys. 107 (2010) 124516.
[4] T. Lauermann, A. Zuschlag, S. Scholz, G. Hahn, B. Terheiden, Proc. 26th EUPVSEC, Hamburg, 2011, 1137.
[5] H. Plagwitz, R. Brendel, Prog. Photovoltaics 14 (2006) 1.
[6] E. Urrejola, K. Peter, H. Plagwitz, G. Schubert, J. Appl. Phys. 110 (2011) 056104.
[7] J. Krause, R. Woehl, M. Rauer, C. Schmiga, J. Wilde, D. Biro, Solar Energy Materials & Solar Cells 95 (2011) 2151.
[8] E. Urrejola, K. Peter, H. Plagwitz, G. Schubert, Appl. Phys. Lett. 98 (2011) 153508.
[9] T. Lauermann, B. Fröhlich, G. Hahn, B. Terheiden, Prog. Photovolt.: Res. Appl., DOI: 10.1002/pip. 2388
[10] R. Preu, S. W. Glunz, S. Schäfer, R. Lüdemann, W. Wettling, W. Pfleging, Proc. 16th EUPVSEC, Glasgow 2000, 1181
[11] J. Specht, D. Biro, N. Mingirulli, M. Aleman, U. Belledin, R. Efinger, D. Erath, L. Gautero, A. Lemke, D. Stüwe, J. Rentsch, R. Preu, Proceedings of Internat. Conf. On Digital Printing Technologies and Digital Fabrication, Pittsburgh PA, 2008, 912
[12] Z. R. Du, N. Palina, J. Chen, F. Lin , M. H. Hong, B. Hoex, Proc. 27th EUPVSEC, Hamburg 2012, 1203.
[13] K. Dressler, S. Dauwe, T. Droste, J. Rossa, R. Meidel, K. Schünemann, K. Ramspeck, Y. Gassenbauer, A. Metz, Proc. 27th EUPVSEC, Hamburg 2012, 755.
[14] X. Meng, J. Wu, J. Xie, X. Wang, L. Zhang, Proc. 28th EUPVSEC, Paris 2013,1562.
[15] T. Fang, C. Lin, K. Li, L. Wang, W. Tang, Proc. 26th EUPVSEC, Hamburg 2011, 2220.